Intermetallics. Vol. 15. Núm. 7. 2007. Pag. 891-900
http://dx.doi.org/10.1016/j.intermet.2006.10.052

Microstructure and Mechanical Properties of Bulk Nanocrystalline $Al_{88}Mm_5Ni_5Fe_2$ Alloy Consolidated at High Pressure

H. Dimitrov[1], J.S. Blázquez[2*], J. Latuch[1], T. Kulik[1]

[1] *Faculty of Materials Science and Engineering, Warsaw University of Technology, Wołoska 141, 02-507 Warsaw, Poland*

[2] *Departamento de Física de la Materia Condensada, Instituto de Ciencia de Materiales, CSIC-Universidad de Sevilla, Apartado 1065, 41080 Sevilla, Spain*

Abstract: Bulk nanocrystalline $Al_{88}Mm_5Ni_5Fe_2$ alloys have been produced by consolidation of pulverised melt-spun ribbons at high pressure. Different production procedures were explored to improve the quality of compaction of the resulting bulk samples. Quality of compaction of samples pressed at room temperature is clearly improved by increasing applied pressure from 2 to 7.7 GPa. All hot compacted samples had good quality of compaction. Onset of crystallisation shifts to higher temperatures as the applied pressure increases. Nanocrystalline powder fails to be compacted at room temperature even at 7.7 GPa. Mechanical properties were studied in terms of Vickers microhardness. Relationship between microhardness and microstructure of bulk samples was studied in the frame of two different theoretical models.

Keywords: A-aluminides (miscellaneous), C-nanocrystals, F-mechanical testing.

* Corresponding author: J. S. Blázquez

Tel.: +34-954559541

Fax: +34-954612097

e-mail: jsebas@us.es

Intermetallics. Vol. 15. Núm. 7. 2007. Pag. 891-900
http://dx.doi.org/10.1016/j.intermet.2006.10.052

1 Introduction

Amorphous Al-based alloys are interesting for their excellent mechanical properties, superior to those of the commercial crystalline Al-based alloys (e.g. tensile strength in amorphous alloys is twice higher compared to commercial crystalline ones) [1]. However, mechanical properties can be still improved in some compositions, exhibiting a primary crystallisation in which nanocrystalline microstructure is developed [2]. This microstructure consists of dispersed nano-sized crystals (~20 nm) of α-Al embedded in a residual amorphous matrix. One successful way for achieving nanocrystalline microstructure is the controlled crystallisation of a precursor amorphous alloy. This amorphous microstructure can be achieved by rapid quenching techniques, e.g. melt-spinning technique, applied to quaternary systems containing Al, rare earth (RE) or Y, and two transition metals (TM) [3].

Although the main interest of Al-based alloys applicability is as bulk samples, the typical procedures for obtaining amorphous or nanocrystalline alloys lead to thin ribbons (melt-spinning, typically tens μm thick) or powder samples (atomisation or mechanical alloying). Therefore, much effort has been devoted to powder consolidation by different procedures, as hot extrusion [4-6], hot pressing [7,8] and cold consolidation using severe plastic deformation [9].

On the other hand, relationship between microhardness and microstructure of nanocrystalline Al-based alloys is not fully understood yet, and different models predict different dependence of microhardness on crystalline volume fraction [10-13].

In this work, different ways of production of bulk nanocrystalline samples were explored and the relationship between hardness and nanocrystalline microstructure was studied. $Al_{88}Mm_{88}Ni_5Fe_2$ alloy was chosen for this study, where Mm denotes Mischmetal, which is a mixture of different lanthanides. The use of Mm highly reduces the cost of the alloy, without big effect on the crystallisation process, with respect to compositions

containing pure rare earth elements [14]. Previous work on the studied composition [15] showed that devitrification process occurs in three different stages. Nanocrystalline microstructure is developed during primary crystallisation (crystallisation onset temperature at 40 K min^{-1}: 514 K), α-Al nanocrystals are embedded into a residual amorphous matrix. A new metastable phase appears during the second crystallisation process and, after the third crystallisation event, final stable phases found are: α-Al, $Al_{11}Mm_3$ and Al_3Ni [16].

2 Experimental

Ingots of quaternary $Al_{88}Mm_5Ni_5Fe_2$ alloy were prepared from pure elements by arc melting in argon atmosphere. Composition of Mischmetal (Mm), in at. %, was: Ce-50.3, La-43.5, Pr-5.9 and Nd-0.3. During melt-spinning, the melt is ejected from the crucible onto a rotating copper wheel at peripheral speeds of 30-40 m s^{-1}. By this technique it is possible to quench the melt at a rate of 10^5-10^6 K s^{-1}. The resulting ribbons were typically 2-3 mm wide and 30-40 μm thick. The melt-spun amorphous ribbons were ball milled in a Fritsch P5 planetary ball mill for 90 min in argon atmosphere at a rotational speed of 250 rpm. Ball to powder ratio was 20:1.

In order to obtain nanocrystalline powder, amorphous ribbons were vacuum-sealed in quartz crucibles and annealed at 508 K in a laboratory tube furnace for 20 min. The resulting nanocrystalline ribbons were ball milled as the amorphous melt-spun ones but for 60 min and the same ball to powder ratio and rotational speed.

A high-pressure toroidal-cell press was used for compacting powders. The powder was initially pre-pressed uni-axially at 100 MPa and the resulting green compact was inserted into the toroidal cell. The shape and the material of the gasket ensure that the compacting conditions are close to isostatic ones. The applied pressures were 2 and 7.7 GPa. Temperatures applied in our experiments were: room temperature (300 K), 548 K and 573 K.

Samples were hold at maximum pressure and room or elevated temperatures for 5 min. Resulting bulk samples are limited to cylinders of 5 mm diameter and a maximum of 5 mm high.

Vickers microhardness measurements were performed on a Zwick hardness tester with a load of 100 g. To improve statistic of the results, 10 measurements were performed on each tested bulk sample (5 on both faces). The surface was previously polished by hand. The error was estimated from the deviation of the set of measurements to be ~±25 HV. During the experiments, the size of the indenter mark was >15 μm.

Quality of compaction of the as-pressed bulk samples was determined by scanning electron microscopy (SEM), in a Hitachi S-3500N equipment, as well as density measurements. SEM observations were performed after hardness tests on polished surface. Besides some of the samples with bad quality of compaction (preventing hardness testing) were also observed by SEM. In such cases, the surface was not polished. Density of compacted bulk samples was determined by Archimedes method using a Gibertini E154 balance with a set for solid state density measurements. Before the samples were subjected to weight measurements, they were kept in boiling water.

Differential scanning calorimetry (Perkin-Elmer DSC7) was used in argon atmosphere for characterising the crystallisation behaviour of amorphous ribbons and powder samples. The same equipment was used for annealing of the bulk samples. The heating rate used was 40 K/min.

Phase composition and microstructure were determined using X-ray diffraction technique (XRD) in a Philips diffractometer operated with Cu Kα wavelength. Crystalline volume fraction (V_{cr}) and average crystalline size were estimated by this technique. To obtain V_{cr}, a deconvolution procedure was performed to separate crystalline peaks and amorphous halo in a 2θ range from 27.5 to 47.5 degrees involving the amorphous halo and the crystalline

diffraction maxima of the α-Al phase (111) and (200) [16]. Crystalline peaks were fitted using Lorentzian function, assuming the small grain size as the main effect contributing to the broadening of the diffraction peaks. Amorphous halo was fitted using a Gaussian function. V_{cr} was estimated from the area ratio between the (111) peak and the sum of (111) peak and the amorphous halo. This area ratio was corrected taking into account the different scattering factor of the Al (which can be assumed as the only element in the crystalline phase [17]) and those of the elements composing the residual amorphous matrix (enriched in Mm, Ni and Fe elements and impoverished in Al), as it is detailed elsewhere for other nanocrystalline systems [18]. The main advantage of this measurement of V_{cr} with respect to the widely used enthalpy fraction from DSC is that, in calorimetric measurements, the difference in the enthalpy associated to the formation of different phases is neglected and possible recrystallisation processes can lead to misleading of the results. The procedure for V_{cr} measurement detailed here is expected to give absolute values of this magnitude with an error below 10 %. Average grain size was estimated using Scherrer's formula. In the present work, the microstrain effects and the possible presence of a grain size distribution were neglected. However, as the approximations are imposed for all the samples studied in the same way, the obtained values are trustworthy as an estimation of the order of the nanocrystal size and an error bar of ±5 nm was assumed.

Bulk samples had a surface smaller than the illuminated area by the X-ray beam. Therefore, special care was taken for positioning of the samples. Before the deconvolution procedure was applied, background was substracted using the registered XRD pattern of the empty holder, specially designed to match the shape of the bulk samples.

3 Results

3.1 Production procedures

Intermetallics. Vol. 15. Núm. 7. 2007. Pag. 891-900
http://dx.doi.org/10.1016/j.intermet.2006.10.052

Figure 1 schematically shows the three ways of production of bulk nanocrystalline material proposed in this work, each of them starting from amorphous ribbons obtained by melt-spinning technique. Figure 2 shows the XRD pattern and DSC scan corresponding to as-cast amorphous ribbons. The three procedures are listed below.

Bulk samples from amorphous powder pressed at room temperature. Amorphous powder was obtained by ball-milling of amorphous ribbons. Figure 3 shows the XRD pattern and the DSC scan of the amorphous powder obtained by milling. The powder was pressed at room temperature at different applied pressures (2 and 7.7 GPa, maximum pressure was applied for 5 min), to obtain bulk amorphous samples. Nanocrystalline microstructure was achieved by subsequent annealing at 508 K (about 5 K below the onset of crystallisation measured at heating rate of 40 K/min [15]) for different times (from 5 to 60 min). Figure 4 shows the XRD patterns of the final nanocrystalline bulk samples after the different annealing processes. The *a priori* advantage of this procedure is that the amorphous state of the powder is preserved during pressing and the nanocrystalline microstructure is achieved by a well controlled annealing process.

Bulk samples from amorphous powder pressed at high temperature. The procedure followed is similar to the previous one, but instead of cold compaction (pressing at room temperature), hot compaction was performed. Therefore, two parameters were changed in these experiments: pressure and temperature of compaction. The time at maximum pressure, which is coincident with the time the sample was submitted to isothermal annealing, was 5 min. Figure 5 shows the XRD patterns of the different samples obtained by this procedure. It can be seen that not all the samples developed a nanocrystalline microstructure, although the pressing temperature was as high as 35 K over the onset temperature registered by DSC at 40 K/min (see Fig. 2b and Fig. 3b). From figure 5 it can be concluded that the onset of crystallisation shift to higher temperature as the applied pressure increases: sample pressed at

548 K and 7.7 GPa has an amorphous XRD pattern, meanwhile sample pressed at the same temperature at 2 GPa evidences clear crystalline peaks corresponding to the α-Al phase, which was analysed after subtraction of the baseline as it is described in the Experimental section. The bulk sample obtained in amorphous state by this procedure was subsequently annealed in the same way as the cold compacted samples to achieve a controlled nanocrystalline microstructure.

The main *a priori* advantage of this procedure is that one extra process could be avoided if the nanocrystalline microstructure is achieved (annealing and pressing are done at the same time). The annealing conditions at which the nanocrystalline microstructure is developed are less controllable than in a furnace. Another important advantage that might be pointed for the hot compacted samples with respect to the cold compacted samples is that high temperature pressing might enhance the quality of compaction of the resulting bulk material, enhancing the binding among powder particles.

Bulk samples from nanocrystalline powder pressed at room temperature. In this case, nanocrystalline microstructure was achieved by annealing of amorphous ribbons at 508 K for 20 min. The nanocrystalline microstructure developed was characterized by a crystalline volume fraction of 0.3 and an average grain size of 19 nm. Afterwards, nanocrystalline ribbons were milled in order to produce nanocrystalline powder, which was compacted at room temperature at two different pressures, 2 and 7.7 GPa. This procedure presents the same advantage as the first procedure and the nanocrystalline microstructure can be finely controlled by annealing the amorphous ribbons. Besides, a new *a priori* advantage appears, because nanocrystalline ribbons present a higher thermal stability than that of the amorphous structures, facilitating that the milling process does not affect the microstructure.

3.2 Quality of compaction

The quality of compaction of the as-pressed samples was checked using SEM and density measurements. Three are the main parameters which could affect the quality of compaction: microstructure of the powder, temperature of pressing and applied pressure.

Figure 6 shows the SEM micrographs of the bulk samples obtained by cold compaction of amorphous powder (the scratches are due to the hand polishing of the samples as they were prepared for hardness testing). Density is also indicated. In this case, only compaction pressure varies. Some individual smashed particles could be observed on the sample pressed at 2 GPa, whereas, for the sample compacted at 7.7 GPa, homogeneous flat surface, indicating a good quality of compaction was observed. Density is also lower in the sample compacted at 2 GPa than in the sample compacted at 7.7 GPa (3.06 and 3.18 g cm^{-3}, respectively). From these results it can be concluded that, in the region explored, pressure has a big effect on quality of compaction, being noticeable the effect of increasing pressure up to 7.7 GPa with respect to 2 GPa for a good compaction at room temperature. This conclusion is worth noticing because the applied pressures are typically below 1 GPa [7,8]. However, sample pressed at 300 K and 2 GPa could be successfully prepared for hardness measurements (it did not become ruined by polishing its surface) and, therefore, it was considered well compacted for further studies.

Figure 7 shows densities and SEM micrographs of the bulk samples obtained by hot compaction of amorphous powder. In this case, the effect of pressing temperature and applied pressure could be studied. All the samples obtained by this procedure showed high density (~3.2 g cm^{-3}) and a flat surface in which the individual particles of the former powder were indistinguishable, as it was observed in the sample compacted at room temperature and 7.7 GPa. The main difference observed was the resulting microstructure of the hot compacted bulk samples. As it was mentioned above, the increase of the applied pressure shifts the onset of crystallisation to higher temperatures: for the same temperature of pressing, 548 K, sample

pressed at 7.7 GPa presented a fully amorphous microstructure, whereas samples pressed at 2 GPa developed nanocrystalline microstructure with ~0.4 crystalline volume fraction and 15 nm of average grain size (see Fig. 5). On the other hand, samples pressed at 2 GPa and different temperatures (548 and 573 K, respectively) for 5 min, show no difference in the final microstructure achieved, both cases presenting the same values of V_{cr} and average grain size. It is worth noticing that, although nanocrystalline microstructure is expected to be denser than amorphous one, the bulk sample which results in amorphous state after hot compaction shows even a slightly higher density than those resulting in nanocrystalline state. Therefore, it might be inferred that the bulk amorphous sample obtained by hot compaction shows the best quality of compaction among the studied samples.

Figure 8 shows densities and SEM micrographs of the bulk samples obtained by cold compaction of nanocrystalline powder. Both samples presented bad quality of compaction and it is possible to distinguish the individual particles of the nanocrystalline powder. Moreover, it was not possible to prepare the samples for hardness measurement, being ruined during surface polishing. However, SEM micrographs and density measurements clearly show that a better compaction, although not successful, could be obtained in the sample pressed at 7.7 GPa. This sample showed higher density in comparison with that exhibited by the sample pressed at 2 GPa and at room temperature from amorphous powder, which was considered to be a successful bulk sample. However, the higher density of the sample obtained from nanocrystalline powder pressed at 7.7 GPa could be explained by its different microstructure, because crystalline structure has a higher density than amorphous one. In conclusion, nanocrystalline powder, which is supposed to be harder than the amorphous one, fails to be compacted at room temperature in the region of pressures explored in this work, meanwhile the less hard amorphous powder could be successfully compacted even at 2 GPa and room temperature.

Intermetallics. Vol. 15. Núm. 7. 2007. Pag. 891-900
http://dx.doi.org/10.1016/j.intermet.2006.10.052

3.3 Hardness measurements

Samples obtained by pressing of amorphous powder at room temperature and at 548 K and 7.7 GPa were amorphous. For these samples, which present the same microstructure, it could be assumed that density becomes the main parameter affecting the mechanical properties. Figure 9 shows the effect of the density on the microhardness values of the amorphous bulk samples. It is clearly seen that hardness increases as density of the bulk samples increases. In our particular case, an increase in density of 7 % (from 2.99 to 3.21 g cm^{-3}) results in an increase of the microhardness of 40 % (from 270 HV=2.65 GPa to 380 HV=3.73 GPa) without change of the microstructure. This indicates that quality of compaction is a very important factor and must be improved to optimise the hardness of the material.

In the case of nanocrystalline samples, other parameters might affect the mechanical properties, specially those characterizing the nanocrystalline microstructure: crystalline volume fraction and grain size. In order to study the relationship between these parameters and microhardness, systematic annealing was performed on the three as-pressed amorphous bulk samples. Isothermal annealing procedures at 508 K for different times (from 5 to 20 min) were applied in order to obtain different microstructures. Microstructure was studied using XRD technique which allows us to estimate the crystalline volume fraction and the average crystal size, as it was indicated in the experimental section. In our particular case, estimated crystal size was between 15 and 20 nm with an error about 5 nm. Grain size could be considered constant so its effect on the microhardness will be neglected. Therefore, discussion on relationship between mechanical properties and microstructure will be focused on the relationship between Vickers hardness and crystalline volume fraction.

Intermetallics. Vol. 15. Núm. 7. 2007. Pag. 891-900
http://dx.doi.org/10.1016/j.intermet.2006.10.052

4. Discussion

Two different models have been developed to explain the relationship between hardness and microstructure. According to the first model, proposed by Zhong et al in 1997 [10], the increase of the hardness, as the crystalline volume fraction of α-Al phase increases, is directly related to the hardening of the residual amorphous matrix because of its enrichment in elements different than Al (solute elements), due to the low solubility of these elements in the α-Al phase, which can be considered close to pure Al [17].

The second model, developed by Kim et al in 1999 [11], although it was used in a previous work [19], is known as the mixture model. Microhardness of the system is obtained as an average of the corresponding to the residual amorphous matrix and the corresponding to the defect-free, and therefore very hard, α-Al nanocrystals. The average is weighted using their respective volume fractions.

Both models are in agreement considering several points:

- hardness increases as the nanocrystallisation progresses;
- nanocrystals' composition is assumed to be pure Al, whereas RE(Y) and TM elements are rejected from the nanocrystals to the amorphous matrix as it has been evidenced by atom probe technique [17];
- nanocrystals of α-Al is the hardest phase, due to its defect-free structure. This defect-free structure leads to the assignation of the theoretical hardness value to the fcc α-Al (816 HV=8.00 GPa [12]);
- hardness of the residual amorphous matrix increases as its composition is impoverished in Al and, therefore, enriched in rare earth and transition metal elements;
- the evolution of the hardness of the residual amorphous versus the solute content (elements different than Al) of the residual amorphous matrix is close to linearity.

The last point was checked for Al-Y-Ni alloys using fully amorphous ribbons which compositions corresponding to those of the residual amorphous matrix enriched in solute content at different values of V_{cr} [10, 11]. On the other hand, both models calculate the crystalline volume fraction from the enthalpy ratio, although it is explicitly recognized that this method is not valid for absolute values of crystalline volume fraction, being however trustable for obtaining relative values of this magnitude [12]. It is worth noticing that in a later paper discussing both models, the effect of nanocrystals would be considered when the percolation limit (V_{cr} ~0.5-0.6) is overcome, but it is assessed that this limit is hardly obtained in Al-based nanocrystalline alloys before the second crystallisation stage takes place [12] (taking into account the procedure of measuring V_{cr}).

The divergences between both methods could be summarized in the predicted dependence of the Vickers hardness as the nanocrystallisation progresses. In the case of Zhong's model, hardness would be linear with the increase of solute content in the residual amorphous matrix (assuming the hardness corresponding to the residual amorphous matrix increases linearly with this parameter). On the other hand, Kim's model (mixture model) predicts a linear increase of the hardness as the crystalline volume fraction increases.

Figure 10 shows the relation between these two parameters for the studied composition, $Al_{88}Mm_5Ni_5Fe_2$. This correlation can be easily obtained once the composition of the initial and one of the two final phases are known (in our case α-Al, which is assumed to be pure Al):

$$C(\beta)_{Ini}=V_{cr}C(\beta)_{Nano}+[1-V_{cr}]C(\beta)_{RA} \quad \text{(i)}$$

Where $C(\beta)_{Ini}$, $C(\beta)_{Nano}$ and $C(\beta)_{RA}$, are the content on β element (Al, Mm, Ni or Fe) in the initial amorphous phase, crystalline phase and residual amorphous matrix, respectively.

As it can be seen in figure 10, relationship between V_{cr} and solute content is difficult to distinguish from a linear behaviour below V_{cr}~0.4, taking into account the error of the

measurements. This fact, together with the ambiguity of the absolute values of the crystalline volume fractions reported from the measurement of the enthalpy ratio, does not give the possibility for good comparison between the two methods because absolute values of V_{cr} are necessary to calculate the solute content of the residual amorphous matrix. Therefore, it is hard to distinguish between the predictions of both models if absolute values of crystalline volume fraction are not obtained.

As it was detailed in the experimental section, the method proposed in this work for the calculation of crystalline volume fraction is assumed to be closer to the real absolute values than the values obtained from the enthalpy ratio, which assume the same enthalpy for transformed fraction independently of the crystallised phase (α-Al or intermetallic phases), or neglect recrystallisation phenomena which could strongly affect the obtained V_{cr} value. However, the values obtained from the enthalpy ratio are widespread extended and considered as valid for relative changes in the same composition [12].

Figures 11a and 11b show hardness versus V_{cr} and solute content, respectively. It can be observed that the increase of hardness is saturated at a certain value of V_{cr} (~ 30 %). This saturation behaviour is in agreement with the close relationship between crystalline volume fraction and microhardness. However, samples nanocrystallised during hot pressing (also shown in Fig.11) present a higher crystalline volume fraction (~0.4 with respect to the ~0.3 maximum value obtained for isothermally annealed samples 60 min at 508 K) but the observed values of microhardness are similar to those obtained in the saturation regime of bulk samples isothermally annealed at 508 K.

For amorphous samples and nanocrystalline at low crystalline volume fraction, it can be observed that density of compaction is a very important parameter. As the crystalline volume fraction increases, microhardness increases and the differences between samples compacted with different densities slightly decrease, although they are still noticeable, and the

maximum hardness (540 HV=5.30 GPa) is obtained for the bulk sample pressed at 7.7 GPa at 548 K from amorphous powder, which exhibits the maximum density after compaction, after being annealed for 20 min at 508 K.

Our data does not show any linear dependence neither with V_{cr} nor with the solute content of the amorphous matrix, but this could be ascribed to a non linear evolution of the microhardness of the residual amorphous matrix with the solute content in our $Al_{88}Mm_5Ni_5Fe_2$ alloy unlike in the Al-Y-Ni alloys [10,11]. Although, for a proper comparison with the two models cited above, it would be necessary to know the hardness values of the residual amorphous matrix, it is possible to compare our data with the predicted limits of the models, taking into account that both agree in a continuous increase of the hardness of the residual amorphous matrix as the crystalline volume fraction increases. Therefore, in the case of Zhong's model, a minimum value will correspond to the value of the amorphous sample. Our data fulfilled this requirement and a continuous increase from the initial value of the amorphous sample is observed up to the saturation value. In the case of Kim's model, or mixture model, hardness of the system is obtained from the following formula:

$$Hv_{system}=Hv_{\alpha\text{-}Al}*V_{cr}+Hv_{Residual\text{-}Amorphous}*(1-V_{cr}) \quad \text{(ii)}$$

Where Hv_{system}, $Hv_{\alpha\text{-}Al}$ and $Hv_{Residual\text{-}Amorphous}$ are the Vickers hardness corresponding to the global system, the α-Al phase (816 HV=8.00 GPa [12]) and the residual amorphous matrix, respectively. The latter value is accepted to increase as V_{cr} increases, therefore, a minimum limit of the predictions of Kim's model will be to consider a constant value for the hardness of the residual amorphous matrix and equal to the value of the initial bulk amorphous sample, $Hv_{Initial\text{-}Amorphous}$:

$$Hv_{system}>Hv_{\alpha\text{-}Al}*V_{cr}+Hv_{Initial\text{-}Amorphous}*(1-V_{cr}) \quad \text{(iii)}$$

These minimum limits are plotted in figure 11a as solid straight lines for the three amorphous samples obtained. It can be seen how values of hardness corresponding to low crystalline volume fractions are below this minimum limit predicted by Kim's model.

One very interesting result is the saturation value observed for the bulk samples after being annealed for 20 min. Even a slight decrease in the microhardness value could be observed for samples annealed for 60 min at 508 K. In fact, the evolution of crystalline volume fraction between 20 and 60 min of annealing at 508 K is very small (smaller than the error bar). Although the microstructure could be considered unchanged in terms of V_{cr} and grain size, between samples annealed 20 and 60 min, a longer annealing time could affect the distribution profile of Mm in the amorphous matrix, enhancing the homogeneity of the composition in the residual amorphous and affecting the hardness value of the system. Figure 12 shows the evolution of V_{cr} (Fig. 12a) and Vickers hardness (Fig. 12b) with the annealing time. The saturation behaviour is observed for both plots, reflecting the close relationship between V_{cr} and microhardness explained above.

The microhardness values obtained in this work, with a maximum of 540 HV=5.30 GPa, are comparable to the best found in other bulk Al-based alloys. However, in other works, these values are achieved for microstructures containing not only amorphous matrix and nanocrystals of α-Al phase but other crystalline phases [7,8]. Values for bulk systems with a microstructure of only α-Al nanocrystals embedded in amorphous residual matrix are around ~375 HV (3.70 GPa) in $Al_{85}Y_8Ni_5Co_2$ powders consolidated at ~500 K and 1.2 GPa [7]. Bulk nanocrystalline Al-based samples obtained by extrusion present much lower values, independently of the appearing phases (200-300 HV~2-3 GPa) [4-6]. Cold consolidation by severe plastic deformation enhances the hardness of Al-Nd-Fe nanocrystalline alloy with respect to hot extruded samples up to values over 300 HV~3 GPa [9]. These differences, disregarding those corresponding to the composition changes, could be ascribed to the

different quality of compaction achieved for the different samples. In fact, it was clearly shown in this work that a change of density in amorphous samples strongly affects the microhardness and therefore special attention might be devoted to enhance the quality of compaction of the consolidated powder to optimise the hardness of the system. Recently, very high values of hardness (>900 HV=8.83 GPa) have been reported for nanocrystalline intermetallic $(AlCu)_3Zr$ and $(AlMn)_3Zr$ after consolidation in pore free bulk samples by spark plasma sintering [20] whereas less compact samples (77 % of density) of similar alloys exhibit only values <350 HV=3.43 GPa) [21].

A larger number of works have been devoted to ribbon samples than to bulk samples of ternary Al-RE(Y)-TM or quaternary Al-RE(Y)-TM1-TM2 alloys [10,11,19,22-27]. In our case, measurement of the hardness of as-cast amorphous ribbons leads to a value of 340±25 HV (3.3±0.2 GPa), which is similar to the values obtained for the amorphous bulks with densities about 3.2 g cm^{-3} (see Fig. 9). Hardness values above 500 HV~5 GPa were reported for nanocrystalline ribbons with compositions Al-Mm-Ni [19], Al-Y-Ni [10] and Al-Gd-Ni [26] alloys. These facts allow us to consider the proposed production procedure promising and worth further developments.

5. Conclusions

In this study, several ways of production of bulk nanocrystalline alloys by high pressure compaction were explored. The effect of different compaction parameters on the characterisation and properties of the final bulk samples were studied. Bulk nanocrystalline alloys were successfully produced with high hardness of above 500 HV~5 GPa. Several conclusions can be established:

- Best compacted samples are those compacted at high temperature.
- Nanocrystalline powder fails to be compacted at room temperature even at 7.7 GPa.

- Pressure (in the range from 2 to 7.7 GPa) clearly affects the quality of compaction and the microhardness of samples pressed at room temperature.
- Crystallisation onset is shifted to higher temperatures as the pressure is increased from 2 to 7.7 GPa.
- Microhardness increases as the density of the amorphous bulk increases.
- Microhardness increases as the crystalline volume fraction of α-Al phase increases, reaching a maximum at about 0.25-0.3 crystalline volume fraction.
- Maximum microhardness was achieved in samples compacted at 548 K and 7.7 GPa (which results in an as-pressed amorphous bulk) after annealing for 20 min at 508 K (540 HV=5.3 GPa). This value is comparative to the maximum values reported for Al-based alloys.

References

[1] A. Inoue, K. Ohtera, A. P. Tsai, T. Masumoto, J. Jpn. Appl. Phys. 27 (1998) L280.

[2] Y. H. Kim, A. Inoue, T. Masumoto, Mater. Trans. JIM. 31 (1990) 747.

[3] J. Latuch, H. Matyja, V. I. Fadeeva. Mat. Sci. Eng. A179-180 (1994) 506.

[4] J. Q. Guo, K. Kita, N. S. Kazama, J. Nagahora, K. Ohtera, Mat. Sci. Eng. A203 (1995) 420.

[5] K. I. Moon, K. S. Lee, J. All. Comp. 291 (1999) 312.

[6] S. J. Hong, B. S. Chun. Mat. Sci. Eng. A348 (2003) 262.

[7] Y. Kawamura, H. Mano, A. Inoue, Scripta Mater. 44 (2001) 1599.

[8] I. Börner, J. Eckert, Scripta Mater. 45 (2001) 237.

[9] A. R. Yavari, W. J. Botta-Filho, C. A. D. Rodrigues, C. Cardoso, R. Z Valiev, Scripta Mater. 46 (2002) 711.

[10] Z. C. Zhong, X. Y. Jiang, A. L. Greer, Mat. Sci. Eng. A226-228 (1997) 531.

[11] H. S. Kim, P. J. Warren, B. Cantor, H. R. Lee, Nanostr. Mater. 11 (1999) 241.

[12] A. L. Greer, Mat. Sci. Eng. A304-306 (2001) 68.

[13] H. S. Kim, Mat. Sci. Eng. A304-306 (2001) 327.

[14] J. S. Blázquez, E. Fazakas, H. Dimitrov, J. Latuch, L. K. Varga, T. Kulik, J. Non-Cryst. Solids, 351 (2005)158.

[15] H. Dimitrov, J. Latuch, T. Kulik, Solid State Phenom. 94 (2003) 71.

[16] J. S. Blázquez, H. Dimitrov, J. Latuch, T. Kulik, Solid State Phenom. 101-102 (2005) 265.

[17] K. Hono, Y. Zhang, A. P. Tsai, A. Inoue, T. Sakurai, Scripta Metall. Mater. 32 (1995) 191.

[18] J. S. Blázquez, V. Franco, C. F. Conde, A. Conde, J. Magn. Magn. Mat. 254-255 (2003) 460.

[19] W. S. Sun, M. X. Quan, Mater. Letters 27 (1996) 101.

[20] S. H. Lee, K. I. Moon, K. S. Lee, Intermetallics 14 (2006) 1.

[21] S. S. Nayak, S. k. Pabi, B. S. Murty, Intermetallics, in press, online 30 May 2006.

[22] T. Gloriant, L. A. Greer, Nanostr. Mat. 10 (1998) 389.

[23] E. S. Humphreys, P. J. Warren, J. M. Tichmarsh, A. Cerezo, Mat. Sci. Eng. A304-306 (2001) 844.

[24] A. Inoue, H. Kimura, J. Light Metals 1 (2001) 31.

[25] M. A. Muñoz-Morris, S. Suriñach, L. K. Varga, M. D. Baro, D. G. Morris, Scripta Mater. 47 (2002) 31.

[26] B. C. Ko, P. Wesseling, O. L. Vatamanu, G. J. Shiflet, J. J. Lewandowski, Intermetallics 10 (2002) 1099.

[27] M. A. Muñoz-Morris, S. Suriñach, M. Gich, M. D. Baro, D. G. Morris, Acta Mater. 51 (2003) 1067.

Intermetallics. Vol. 15. Núm. 7. 2007. Pag. 891-900
http://dx.doi.org/10.1016/j.intermet.2006.10.052

Figure captions

Figure 1: Scheme of the three different ways of production followed for obtaining bulk nanocrystalline alloys.

Figure 2: (a) XRD pattern and (b) DSC scan, registered at 40 K/min, of amorphous ribbon of $Al_{88}Mm_5Ni_5Fe_2$ alloy.

Figure 3: (a) XRD pattern and (b) DSC scan, registered at 40 K/min, of amorphous powder of $Al_{88}Mm_5Ni_5Fe_2$ alloy.

Figure 4: XRD patterns, after substraction of the background (see experimental section), and fitting curves of $Al_{88}Mm_5Ni_5Fe_2$ alloy obtained by cold compaction at 7.7 GPa and different annealing times at 508 K.

Figure 5: XRD patterns, before substraction of the background (see experimental section), of $Al_{88}Mm_5Ni_5Fe_2$ alloy obtained by hot compaction in their as-pressed state. Conditions of pressing are indicated for each sample.

Figure 6: SEM micrographs of cold compacted $Al_{88}Mm_5Ni_5Fe_2$ alloy from amorphous powder. Density and conditions of pressing are indicated.

Figure 7: SEM micrographs of hot compacted $Al_{88}Mm_5Ni_5Fe_2$ alloy from amorphous powder. Density and conditions of pressing are indicated.

Figure 8: SEM micrographs of cold compacted $Al_{88}Mm_5Ni_5Fe_2$ alloy from nanocrystalline powder. Density and conditions of pressing are indicated.

Figure 9: Vickers microhardness versus density for bulk amorphous samples.

Figure 10: Theoretical relationship between the concentration of the different elements (Al, Mm, Ni and Fe) as well as the solute content (Mm+Ni+Fe) in the residual amorphous matrix and the crystalline volume fraction for the composition $Al_{88}Mm_5Ni_5Fe_2$. Pure Al was considered for α-Al phase.

Intermetallics. Vol. 15. Núm. 7. 2007. Pag. 891-900
http://dx.doi.org/10.1016/j.intermet.2006.10.052

Figure 11: Vickers microhardness versus (a) crystalline volume fraction and (b) solute content in the residual amorphous matrix. Solid lines in (a) represent the minimum limit predicted by the mixture model for each initially amorphous sample. Dashed lines are a guide to the eye.

Figure 12: (a) Crystalline volume fraction versus the annealing time at 508 K and (b) Vickers microhardness versus annealing time at 508 K for bulk $Al_{88}Mm_5Ni_5Fe_2$ alloy. The samples were amorphous in as-pressed state. Lines are a guide to the eye.

Intermetallics. Vol. 15. Núm. 7. 2007. Pag. 891-900
http://dx.doi.org/10.1016/j.intermet.2006.10.052

Figure 1

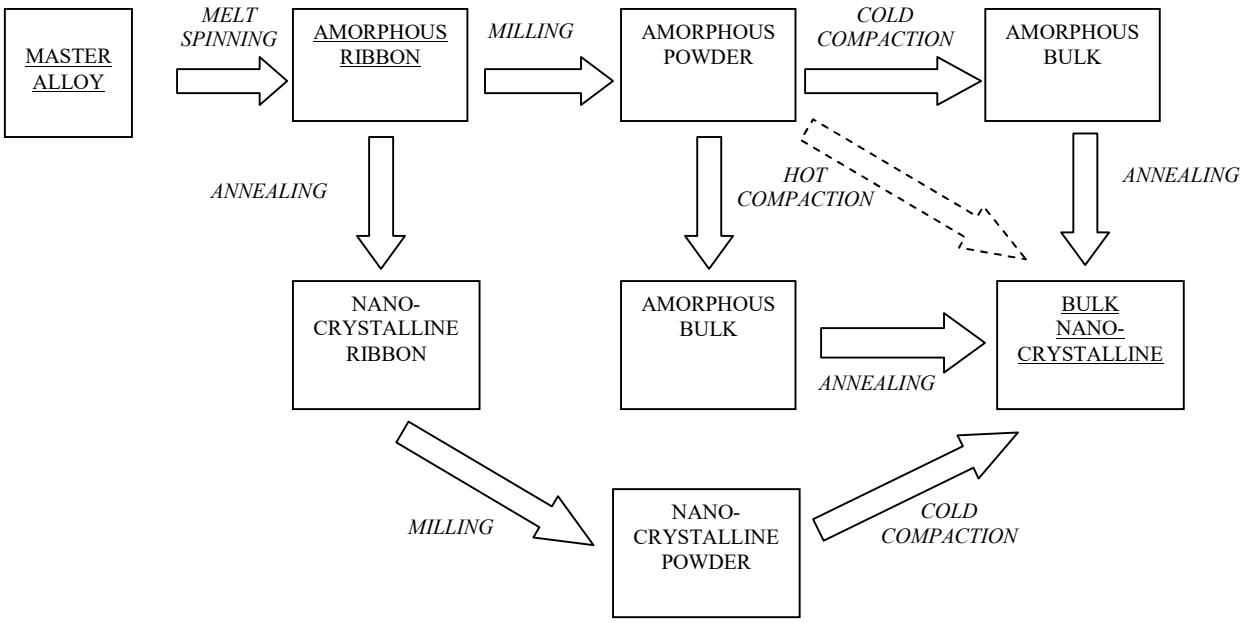

Intermetallics. Vol. 15. Núm. 7. 2007. Pag. 891-900
http://dx.doi.org/10.1016/j.intermet.2006.10.052

Figure 2

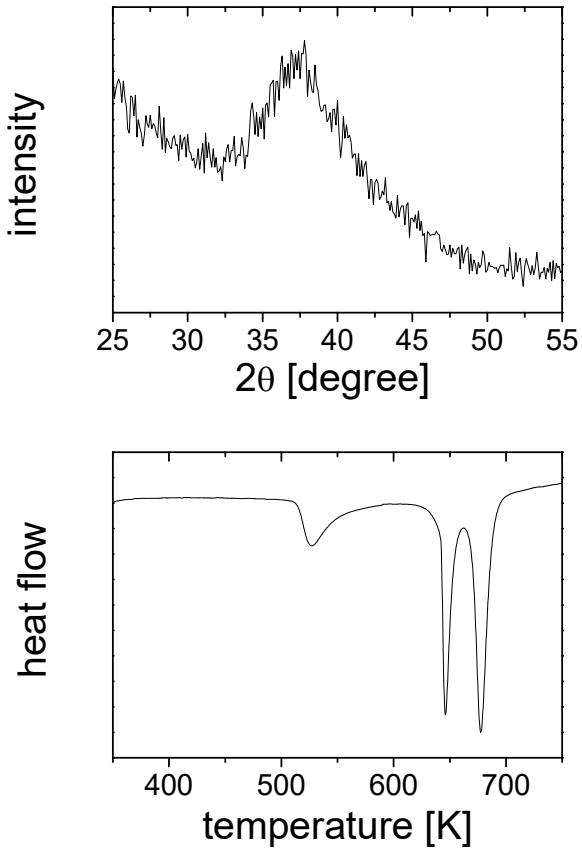

Intermetallics. Vol. 15. Núm. 7. 2007. Pag. 891-900
http://dx.doi.org/10.1016/j.intermet.2006.10.052

Figure 3

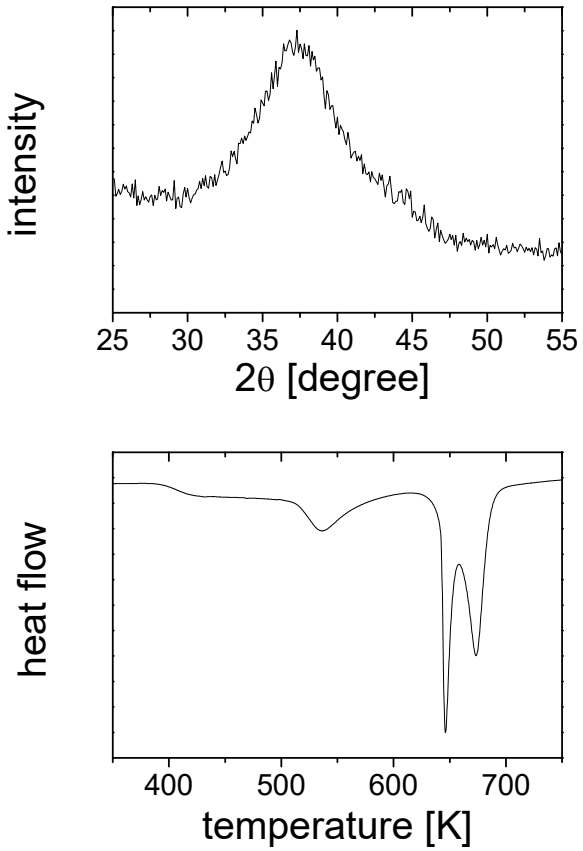

Intermetallics. Vol. 15. Núm. 7. 2007. Pag. 891-900
http://dx.doi.org/10.1016/j.intermet.2006.10.052

Figure 4

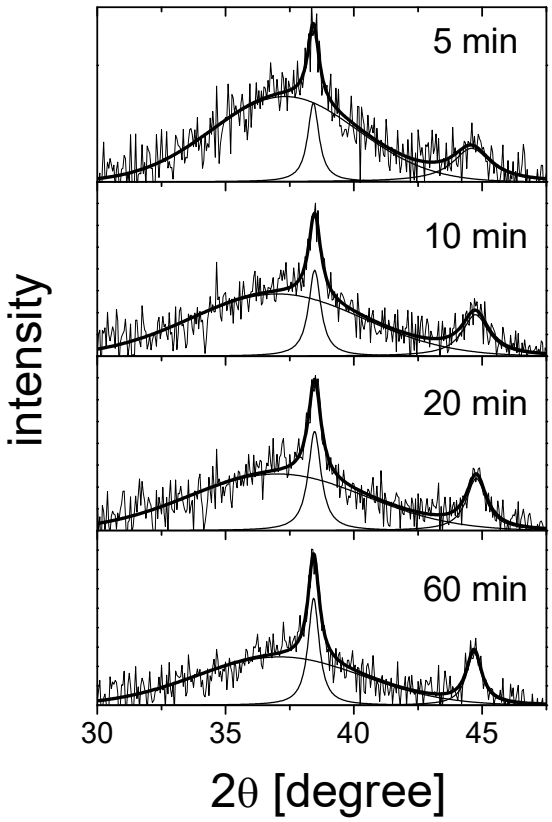

Intermetallics. Vol. 15. Núm. 7. 2007. Pag. 891-900
http://dx.doi.org/10.1016/j.intermet.2006.10.052

Figure 5

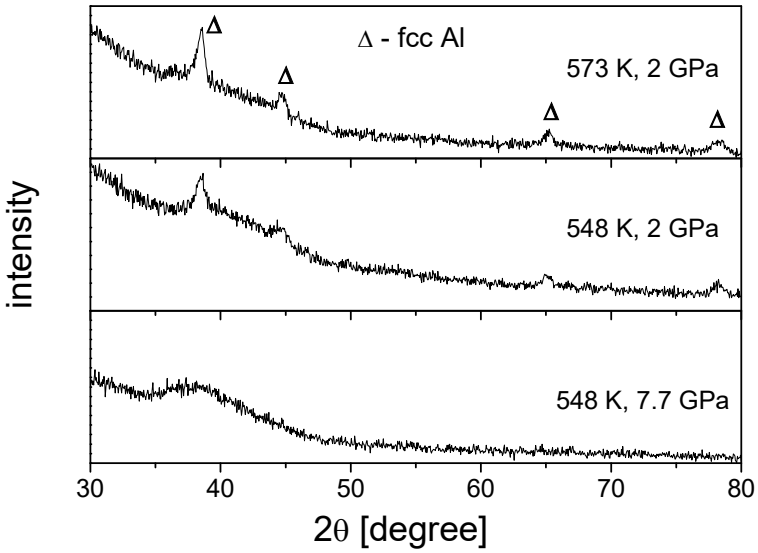

Intermetallics. Vol. 15. Núm. 7. 2007. Pag. 891-900
http://dx.doi.org/10.1016/j.intermet.2006.10.052

Figure 6

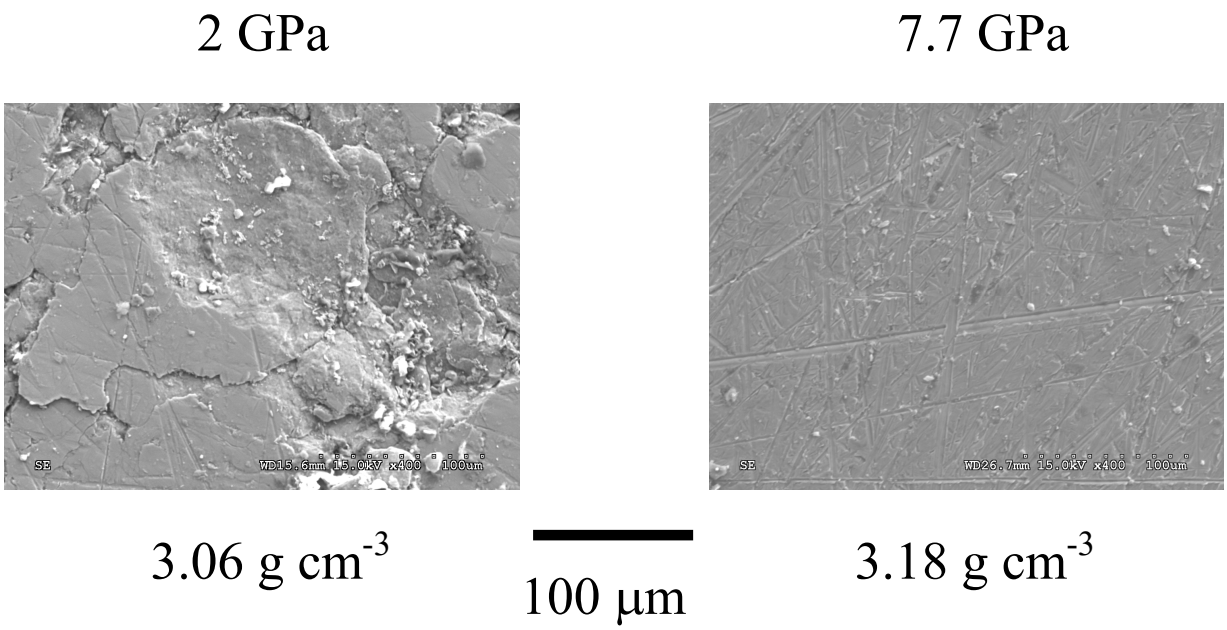

Intermetallics. Vol. 15. Núm. 7. 2007. Pag. 891-900
http://dx.doi.org/10.1016/j.intermet.2006.10.052

Figure 7

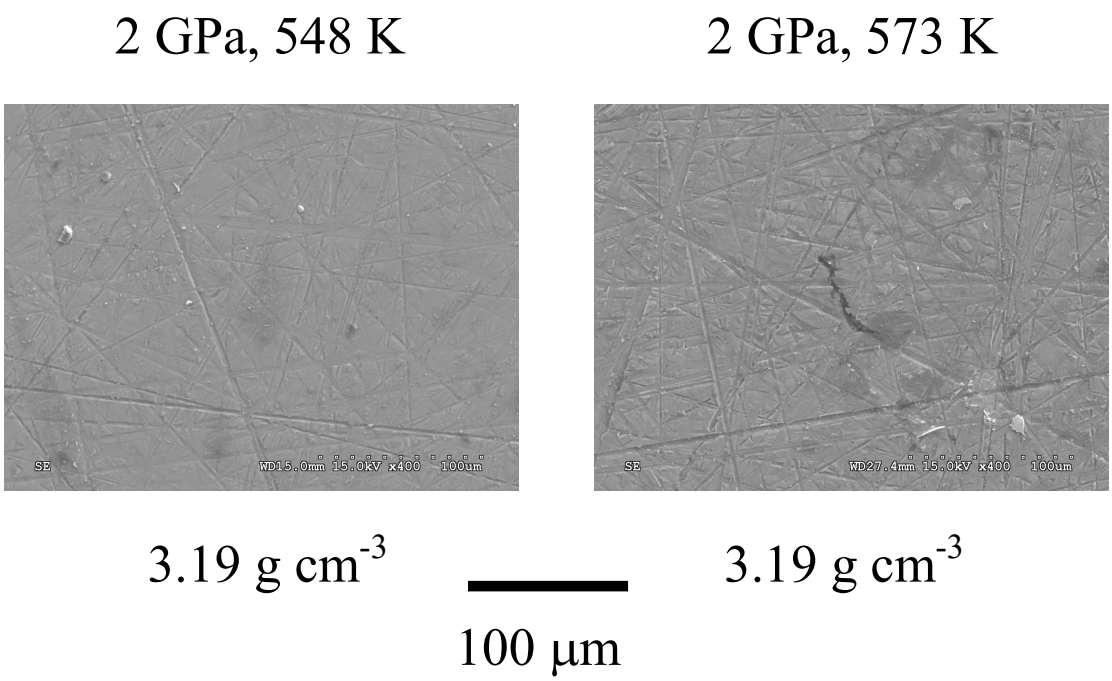

Intermetallics. Vol. 15. Núm. 7. 2007. Pag. 891-900
http://dx.doi.org/10.1016/j.intermet.2006.10.052

Figure 8

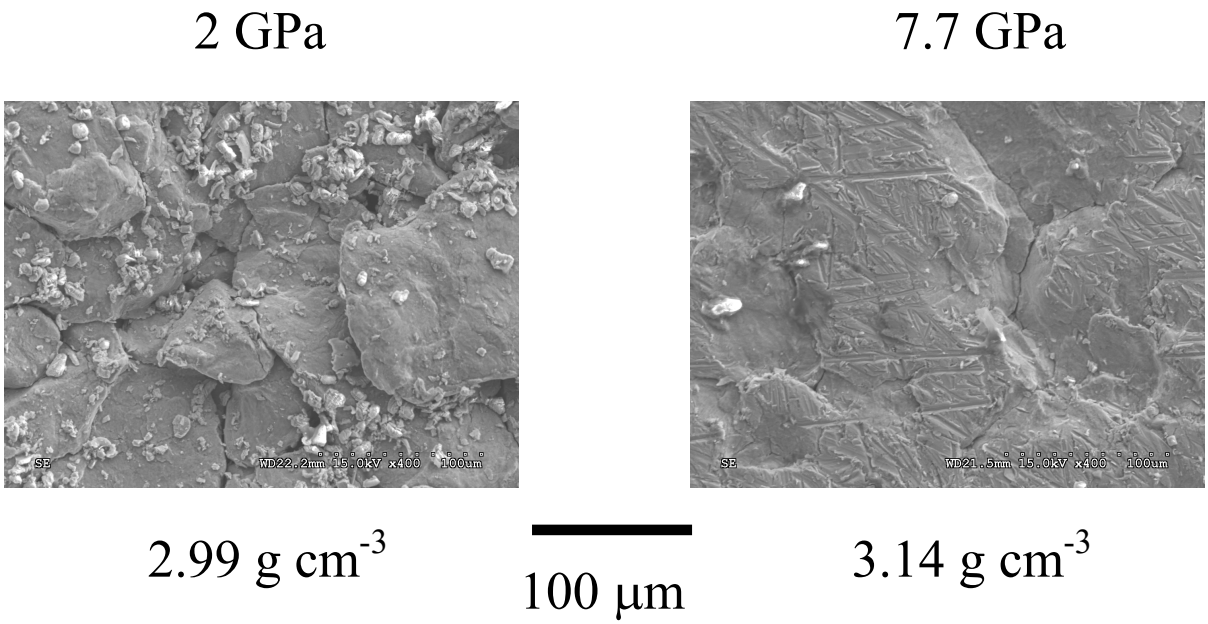

Intermetallics. Vol. 15. Núm. 7. 2007. Pag. 891-900
http://dx.doi.org/10.1016/j.intermet.2006.10.052

Figure 9

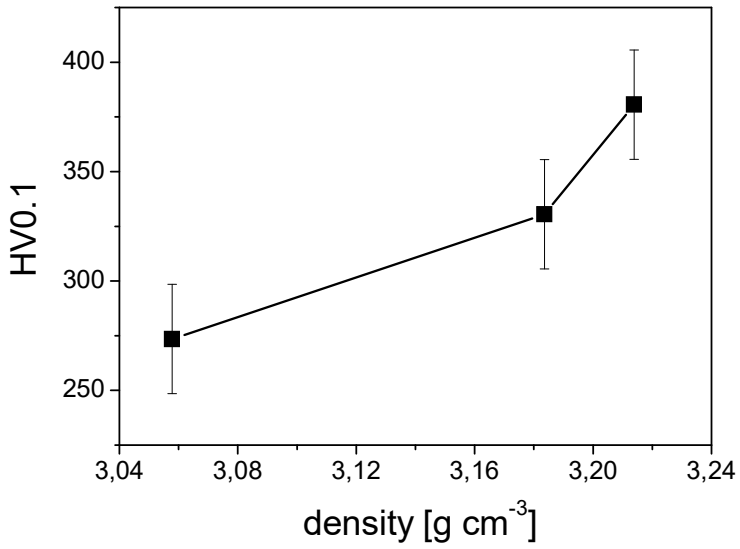

Intermetallics. Vol. 15. Núm. 7. 2007. Pag. 891-900
http://dx.doi.org/10.1016/j.intermet.2006.10.052

Figure 10

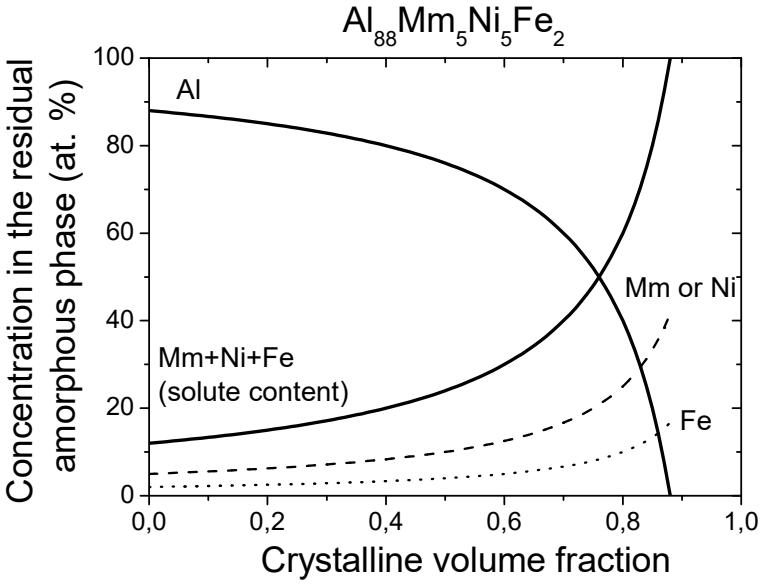

Intermetallics. Vol. 15. Núm. 7. 2007. Pag. 891-900
http://dx.doi.org/10.1016/j.intermet.2006.10.052

Figure 11

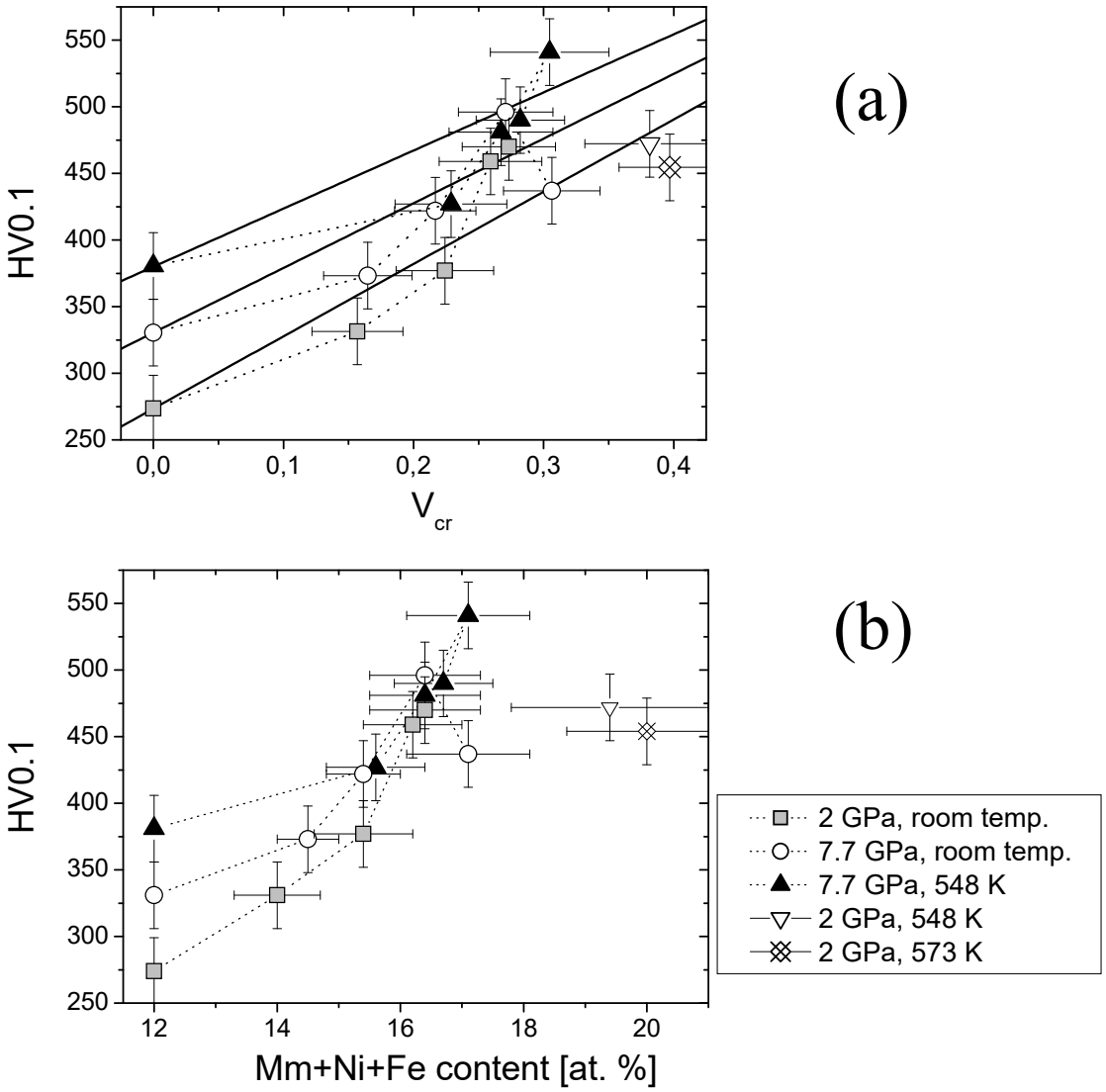

Intermetallics. Vol. 15. Núm. 7. 2007. Pag. 891-900
http://dx.doi.org/10.1016/j.intermet.2006.10.052

Figure 12